Journal of The Electrochemical Society, **149** (8) C396-C405 (2002)
0013-4651/2002/149(8)/C396/10/$7.00 © The Electrochemical Society, Inc.

Monte Carlo Simulation of the Electrodeposition of Copper

I. Additive-Free Acidic Sulfate Solution

Timothy J. Pricer,[a,*] Mark J. Kushner,[b] and Richard C. Alkire[c,,z]**

[a]*IBM Burlington Plant, Essex Junction, Vermont 05452, USA*
[c]*Department of Chemical Engineering and Frederick Seitz Materials Research Laboratory,* [b]*Department of Electrical and Computer Engineering, University of Illinois, Urbana, Illinois 61801, USA*

Simulation of copper electrodeposition on an initially flat surface by a classic two-step electron transfer sequence accompanied by surface diffusion was carried out by a three-dimensional (3-D) kinetic Monte Carlo model linked to a 1-D (continuum) finite difference model. The evolution of deposit roughness was simulated numerically and compared, through use of scaling parameters, with experimental data obtained by atomic force microscopy from deposits formed under constant potential in aqueous solutions of 0.5 M Cu_2SO_4 and 1.0 M H_2SO_4. The model was used to carry out parametric investigations on the effect of adsorption, surface diffusion, and lattice incorporation, all of which were found to exert an influence on the evolution of surface roughness.
© 2002 The Electrochemical Society. [DOI: 10.1149/1.1488648] All rights reserved.

Manuscript submitted February 1, 2001; revised manuscript received February 4, 2002. Available electronically June 21, 2002.

Electrochemical metal deposition involves phenomena that are important at the same time over at widely different time and length scales. For example, the macroscopic current and potential field distribution over a plated part depends upon heterogeneous and homogeneous reactions that occur among various species that move by migration in a potential field, diffusion in concentration fields, and convection in hydrodynamic flow patterns.[1] At the same time, critically important phenomena are associated with nucleation and growth events that occur at the atomic-to-nanoscale at and near the active surface.[2] Indeed, for more demanding small-scale applications such as in the microelectronics field,[3-5] control over molecular aspects of growth morphology is critically important for technological success.

In general, macroscopic engineering models of electrochemical systems do not attempt to describe the rich near-surface chemistry, detailed reaction mechanisms, or intricate molecular traffic patterns that occur in the course of metal ion reduction and lattice formation.[6,7] Accurate description of such events requires noncontinuum methods that can simulate behavior at length scales where the continuum equations of macroscopic engineering models are not valid. At the same time, there have been truly significant advances in experimental techniques that are leading to improved fundamental scientific understanding of molecular mechanisms involved in the electrodeposition process.[8,9] It is important to integrate new molecular knowledge into engineering methods for predicting behavior, as well as design, optimization, and process control. Improved simulation procedures are therefore needed to bridge multiple length scales that are simultaneously important at molecular and macroscopic levels. In the present work, we report on a noncontinuum Monte Carlo model linked to a continuum model to investigate a relatively simple hypotheses of mechanism. The numerical simulation was used to test the hypothesis by comparing experimental roughness evolution data on initially flat surfaces with simulations of deposit growth.

There are several hypotheses of the molecular events that occur when a metal ion moves from a bulk aqueous solution to a surface where it undergoes electrochemical reaction to become incorporated in a metal deposit. For example, a number of investigators have presented experimental studies supporting the importance of surface diffusion in the deposition process[10-15] while others[16-19] favor a mechanism where the metal ion adsorbs and incorporates at the kink sites directly from solution. It has also been suggested[20] that surface diffusion plays a factor only at very low overpotentials. The testing of such hypotheses is difficult when critical parameters are not easily directly measured, such as the surface diffusion coefficient, so that indirect inferences from experimental outcomes are required.

A variety of simulations based on Monte Carlo methods have been developed to investigate the evolution of lattice formation at the atomic level.[21,22] These simulate crystal growth on the time scale associated with surface diffusion and adsorption,[23-26] and have been used in electrodeposition and dissolution to study adsorption,[27-31] morphology evolution in two-dimensional, (2-D)[32-40] and 3-D,[41,42] and 2-D texture formation.[43,44] In general, these works have focused on individual steps of overall reaction mechanisms, rather than on overall mechanisms that consist of a variety of steps and pathways.

There are several indirect experimental methods that are used to test hypotheses of molecular behavior at and near surfaces, of which three found use in this work. Atomic force microscopy (AFM) is used to obtain images of surface roughness that can be qualitatively compared to simulations.[37,45,46] The variation of current with time during constant potential electrolysis is used to identify growth mechanisms based on continuum models[47] as well as noncontinuum models provided that they involve only elements that do not depend on potential. In addition, scaling analysis of the time- and lateral-distance-dependence of the interfacial width, defined as the root-mean-square (rms) of the surface height and obtained experimentally from AFM, images of deposit roughness, provides a quantitative method to evaluate morphology evolution at a surface.[48,49]

In the present two-part work, we investigated reaction mechanisms that are based on adsorption, followed by a two-stage electron transfer sequence that is accompanied by surface diffusion.[50] In this paper Part I, we describe a noncontinuum Monte Carlo simulation of the mechanism that is linked to a continuum model that describes the bulk region. The linked codes were used to predict specific outcomes in pristine experiments, to establish values of the parameters, and to carry out parametric studies. In Part II, we extend the model to include the effect of a simple additive species, and also to use the model to predict shape evolution in additional geometries associated with filling of submicrometer trenches. A more detailed description can be found elsewhere.[51]

Experimental

To obtain a baseline for calibrating and validating the model, copper electrodeposition experiments were performed. Solutions of 0.5 M Cu_2SO_4 and 1.0 M H_2SO_4 were prepared from copper(II) sulfate pentrahydrate (Aldrich, 99.999%), double distilled sulfuric acid (Aldrich), and Millipore-Q purified water (18.0 MΩ cm). The working electrode was a Cu(111) single crystal disk (1 cm diam, Monocrystals Co.) mechanically polished with cloth covered wheels containing 1 and 0.3 μm alumina (Buehler). The counter and reference electrodes were a Pt wire and a Cu wire, respectively. The electrochemical cell consisted of a recrystallization dish where the

* Electrochemical Society Student Member.
** Electrochemical Society Fellow.
[z] E-mail: r-alkire@uiuc.edu

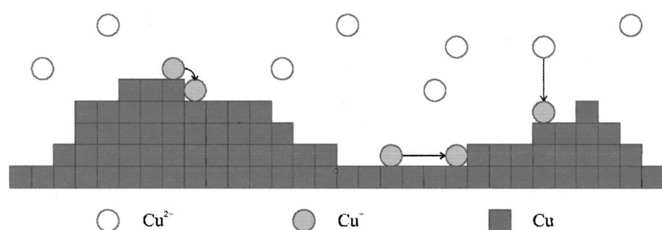

Figure 1. Schematic representation of the hypothetical copper system.

stationary working electrode was pulled above the solution surface by about 0.3 cm to form a hanging meniscus.[52,53] Experiments were carried out at constant potential (Solartron 1286). After electrolysis, AFM images of the electrodeposited metal were obtained (Digital Instruments Nanoscope E AFM, 120 μm scanning head, with Si_3N_4 tips on 200 μm triangular wide leg cantilevers with a force constant of 0.12 N/m). Experiments were conducted *ex situ* to the AFM because there was not enough volume in the AFM fluid cell for the duration of the experiments used here (up to 4×10^3 s), and because the AFM fluid cell configuration was not designed for a uniform current distribution.

The experimental cell was tested to see how well it conformed to a linear 1-D diffusion cell that was the configuration used in the continuum model. Experiments at high potential for which the surface concentration was nearly zero gave a time dependence for the current of $t^{-0.51}$ over 100 s which may be compared with the value of $t^{-0.50}$ for linear diffusion showing that the experimental cell provided nearly linear diffusion. We discuss below the effect of migration, which may have contributed to the difference in slope.

To remove warping caused by the piezoelectric, AFM images were flattened with use of an order of 3 in the x and y directions. Flattened images were analyzed in order to determine how the interface width, defined as the rms of the surface height, scaled in both length and in time.[49] Scaling analysis of the interface width is typically used in connection with the self-affine scaling laws so the experimental results can be compared to continuum equations of growth. In the present investigation, experimentally measured scaling results were compared directly with simulated results, so that self-affinity was not a requirement for use of the scaling analysis method.

Reaction Mechanism for Cu Electrodeposition

A schematic representation of the reaction mechanism of copper electrodeposition used by the Monte Carlo model in this paper is shown in Fig. 1. The basic hypothesis was that Cu^{2+} ions diffuse to the reactive surface where they react by a two-step electron transfer process. The first step involves adsorption of Cu^+ onto the surface

$$Cu^{2+} + e^- \rightarrow Cu^+ \qquad [1]$$

The cuprous adions move by surface diffusion to a second location where they react to become incorporated into the crystal lattice

$$Cu^+ + e^- \rightarrow Cu \qquad [2]$$

The parameters used in the base case calculations were obtained as follows. The bulk diffusion coefficient was taken from the work of Bortels *et al.*[54] Remaining parameters were estimated by taking values from the literature as a starting point (although the experimental conditions were often different from those used in the present work) and then adjusting them further to fit three types of experimental data: AFM images, scaling data that consisted of interface width-time curves obtained from AFM data, and current *vs.* time experimental data.

The initial values used for estimating the Cu^{2+} adsorption rate were based on published values for Cu deposition.[54-56] For the first electron transfer, a transfer coefficient for a reversible system of 0.5

Table I. Monte Carlo Cu model parameters.

Parameter	Value
Cu^{2+} bulk diffusion rate	6.0×10^8 nm²/s
Cu^{2+} adsorption rate	75 nm/s
Cu^{2+} adsorption transfer coefficient	0.339
Cu^+ surface diffusion rate	2.0×10^8 nm²/s
Cu^+ step energy barrier	-1.5×10^{-20} J
Cu^+ broken face energy barrier	-5.0×10^{-22} J
Cu^+ new face energy barrier	5.0×10^{-22} J
Cu^+ incorporation rate	2.0×10^4 nm/s
Cu^+ incorporation transfer coefficient	−0.4
Cu^+ incorporation transfer coefficient Contributions from Cu	0.2

was used. An initial estimate of the Cu^+ surface diffusion coefficient was taken the work of Rynders.[13] The rate of Cu^+ incorporation was assumed to be 1000 times faster than Cu^{2+} adsorption.[57,58] The ease of incorporation of an atom at various types of surface sites was assumed to follow the hierarchy of kink > step > flat surface. To simulate more rapid incorporation at kink sites, a lower transfer coefficient was chosen with each additional Cu neighbor thereby raising the value of the transfer coefficient. The energy barriers for surface diffusion were initially estimated to be 1 kT (4×10^{-21} J) with the value for step movement to be higher.

The parameters obtained for the base case by this procedure are given in Table I. The purpose of establishing a set of values for a base case was to produce a simulation result that resembled three types of pristine experiments. Additional calculations were then carried out with controlled variation of parameters in order to determine the impact on predicted deposition properties.

Method of Solution

The numerical model consisted of a noncontinuum Monte Carlo simulation linked to a continuum model. The linkage consisted of having the Monte Carlo simulator provide a concentration at the interface between the kinetic and continuum regimes for use by the continuum model. The continuum model, in turn, was used to provide a flux at the interface to the Monte Carlo simulator.

Monte Carlo simulation.—The Monte Carlo portion of the integrated model consisted of a 3-D kinetic algorithm that simulated the surface region including a portion of the solution near the surface. The simulation space was represented by a cubic lattice having periodic boundary conditions on the lateral x and y faces, an impenetrable surface on the bottom z face, and an interface to the continuum model on the top z face. The initial position of the surface was located on the bottom face of the simulation space. The simulation was developed in a general manner so that the initial surface can be of any geometry. In the present work, a flat surface is considered in Part I, and a trench is considered in Part II. The cubic lattice of the simulation space was represented internally by a 3-D matrix of integers whose value determined the identify of the material at that location.

Species in the simulation space were represented by blocks in the cubic lattice, referred to in the following paragraphs as particles, an approach that has been used in other applications where mesoscale blocks are used to approximate molecular characteristics.[59,60] These include applications such as use of (atomic scale) Morse potentials to characterize sticking coefficients of blocks during Cu physical vapor deposit,[61] and use of atomic reaction particles in conjunction with direct simulation Monte Carlo for reactive gas dynamics.[62] As indicated in Fig. 1, particles can represent species in solution, adsorbed species and solid species. In the present example, these correspond to Cu^{2+} in solution, Cu^+ adsorbed on the surface and Cu as a solid, respectively. In the present work, the actions a particle may

perform included adsorption, desorption, diffusion in the solution phase, diffusion along the surface, reaction with or without charge transfer, lattice incorporation, and dissolution.

Bulk diffusion was modeled by a random walk mechanism where the particle was allowed to move a distance of one block in a random direction. The actual mean free path between collisions is typically less than one lattice spacing. With bulk diffusion, the particle is capable of moving to one of its six nearest neighbors. The frequency of the random walk is found from[42]

$$f = \frac{6D_b}{L_b^2} \quad [3]$$

All symbols used in equations are defined in the List of Symbols.

Surface diffusion was modeled by a random walk mechanism that took account of the nature of the surface. The frequency of the random walk was taken as[63]

$$f = \frac{6D_s e^{\Delta E/kT}}{L_b^2} \quad [4]$$

The value of the energy barrier was made to be dependent on the local environment of the diffusion path by taking consideration of the factors involved in the energy barrier. These energy barriers included such events as (*i*) the separation of one block from another on the surface such as occurs during surface diffusion of one of them (the ''broken face energy barrier''), (*ii*) the joining of two blocks when one makes contact with another (the ''new face energy barrier''), and (*iii*) the movement along a surface and/or movement between vertical levels such as when cuprous ions adsorb on top of an exposed block and then move down onto the surface to diffuse elsewhere (the ''step energy barrier''). These energy barriers may be positive or negative, depending on whether the surrounding features serve to inhibit or accelerate the processes.

The reaction mechanism allowed a particle to change from one particle type to another type with or without charge transfer, and was used in the present work to simulate adsorption as well as surface reaction involving lattice incorporation. The frequency of a reaction was found from combination of Arrhenius and Tafel-style kinetics[26]

$$f = \frac{Nk_{rxn}e^{(\Delta E/kT \cdot anF\eta/RT)}}{L_b} \quad [5]$$

The reaction can also be conditional on whether the particle is on a surface and/or a conductor. The neighbors of the reacting particle can also affect the reaction kinetics by raising or lowering the energy barrier of the reaction.

By definition, Monte Carlo simulations involve random numbers to determine when and if a particle will make a certain move. Each move for each species has a certain probability associated with it, depending on the time step. There are two time steps that are tracked in the Monte Carlo model. One is the time step over which the continuum code is called for updated flux information; this value is explicitly defined by the user. The second is the Monte Carlo time step, which is not explicitly specified by the used and is computed in the code. Because the Monte Carlo time step must be sufficiently small to capture the full dynamics of the system, the time step is selected to follow the action of the fastest species. To compute the time step, possible frequencies for the actions of each species are computed, and the inverse of each summed frequency is computed. The Monte Carlo time step is chosen to be the smallest inverse summed frequency as shown in Eq. 6 and 7

$$t_{MC_j} = \left(\frac{1}{\sum_{i=1}^{k} f_i} \right)_j \quad [6]$$

$$t_{MC} = \min(t_{MC_j}) \quad [7]$$

where f_i is the frequency, j is the number of species simulated, k is the number of actions for species j, t_{MC_j} is the Monte Carlo time step for species j, and t_{MC} is the Monte Carlo time step selected as the minimum of all t_{MC_j}. In Eq. 6, it can be seen that the Monte Carlo time step is a strong function of the fastest moving species and can thus be approximated as the inverse of the largest frequency in the system. In this work, a typical Monte Carlo time step was 2.8 $\times 10^{-6}$ seconds for a potentiostatic trench filling simulation with a block size of 100 nm, which corresponds to 3.6×10^8 time steps during the simulations.

Once the Monte Carlo time step was computed, then the probability array was constructed for each possible move by each species[26]

$$\bar{\rho}_j = t_{MC} \sum_{i=1}^{k} f_i \quad [8]$$

where $\bar{\rho}_j$ is the probability array for species j that contains a vector of probability bands. If all of the elements of $\bar{\rho}_j$ are summed, then the value of the summation will be less than 1 for all species except the fastest reacting species in the system. If the summation is less than 1, then there is a nonzero probability of rejecting moves in the code for all species except the fastest reacting species in the system. In Eq. 8, each $f_i t_{MC}$ defined a ''probability band'' or bounds on an action. To determine what move a particle is going to make during a certain time step, the probability band (which is between 0 and 1) was compared with a random number (between 0 and 1) and if the random number was greater than the probability band, then the particle ''does nothing'' during that time step. We did not track the number of times a particle does nothing in this investigation.

At each time step, all the particles that could perform actions were checked to see if they performed an action, the data matrix was updated after each action, and when all the particles attempted to perform an action the clock was incremented and the processes was repeated.

Random numbers were obtained from a long period ($>2 \times 10^{18}$) random number generator of L'Ecuyer, with Bays-Durham shuffle.[64,65] Each process requiring a random number used a separate generator with different seed number. The random number generator was used for its long period and speed of computation.

Continuum model.—An elementary 1-D continuum model was used to simulate diffusion in the bulk solution at a distance from the surface. Although more complex codes could have been chosen for this first level implementation, diffusion alone was selected because the Monte Carlo simulation did not include migration and, moreover, a 1-D code was selected because multidimensional effects in the bulk region were not of interest in the present work. The 1-D continuum model consisted of an explicit finite difference solution to the diffusion equation

$$\frac{\partial C}{\partial t} = -D_b \frac{\partial^2 C}{\partial z^2} \quad [9]$$

The boundary conditions consisted of a ''surface'' concentration at the interface to the Monte Carlo simulator that was set at each time increment ($C_{z=0} = C_{MC}$), and a constant concentration boundary condition in the bulk ($C_{End} = C_{Bulk}$).

Computations.—Figure 2 illustrates how information flowed between continuum and noncontinuum models, as well as the sequence by which the foregoing steps were carried out for each particle associated with the Monte Carlo calculations. The code was written in Fortran90 and was run on an SGI Origin 2000. Although the code was parallelized, all of the simulations presented in this work were performed on a single processor as the speedup was less than linear with the number of processors due to gather/scatter operations. In the Monte Carlo simulation, the initial surface geometry consisted of

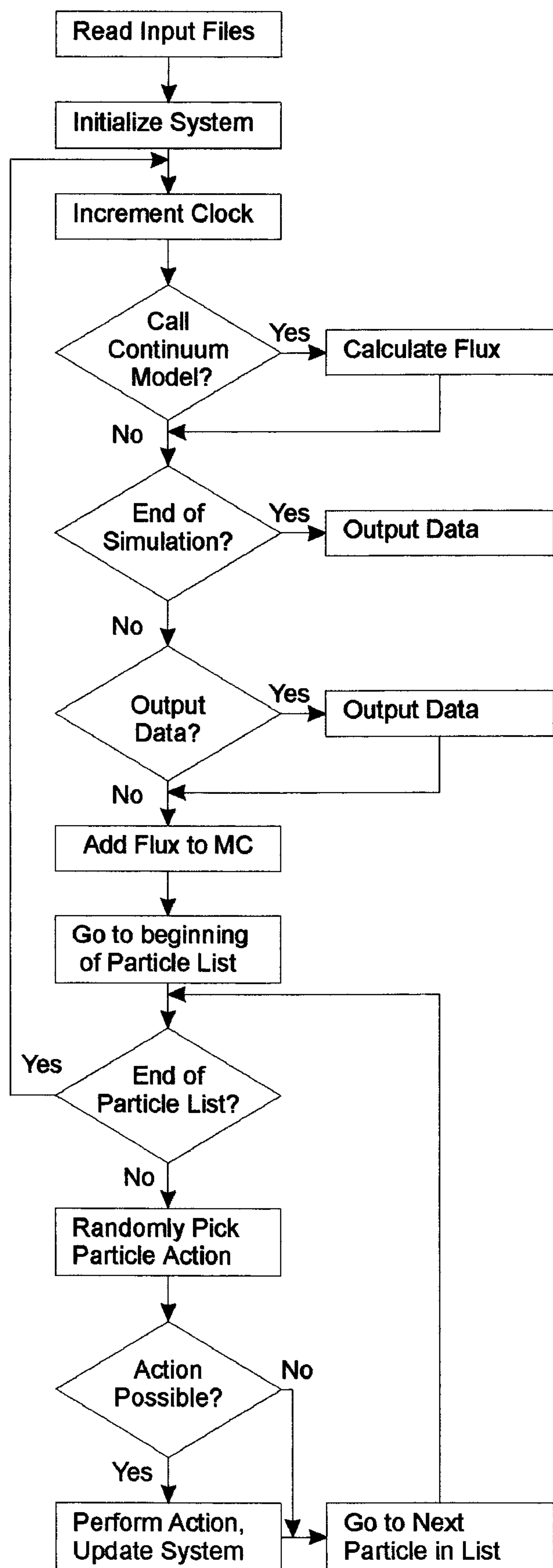

Figure 2. Flow chart of Monte Carlo model.

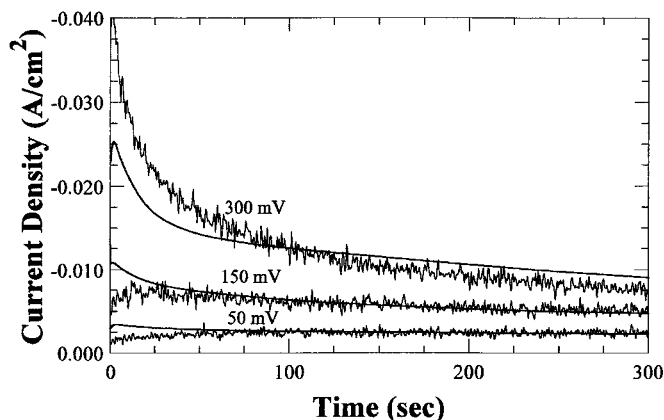

Figure 3. Experimental and simulated currents for Cu deposited at 50, 150, and 300 mV. Smooth curves are experimental and the curves with noise are simulated.

a flat surface that was 100×100 blocks in size; individual block size was 100 nm. The spacing of the z nodes in the continuum code was irregular, starting with small increments near the Monte Carlo interface and increasing toward the bulk solution. Forty nodes were used with the first five nodes being spaced 600 nm apart and with each additional node being 20% larger than the last node. The exchange of information between noncontinuum and continuum codes took place at time intervals of constant size because of stability constraints on the explicit finite difference continuum model although this was not a rate limiting consideration. A typical trench filling simulation had a time step of 2.78×10^{-6} s and required 3.6×10^{8} time steps. A typical simulation took four days to run on a 195 MHz R10000 processor and occupied less than 10 Mb of memory.

From limited experience with this model and other related work, the effect of system size (*i.e.*, 10×10 μm *vs.* 5×5 μm) for the same particle size was that the smaller system took less computational effort, the effect was nonlinear, and other changes in the program could have a comparable effect on simulation time as a fourfold change of electrode area. The effect of particle size for a fixed system size was found not to have an effect on the computed scaling parameters that characterized the rms surface height distribution. The effect of increasing the number of particles for a fixed system size was found to increase the time required for simulation in a nonlinear manner. Our experience suggested that the code should port well to other systems.

Simulations of Copper Deposition

Cu electrodeposition onto a flat surface was simulated numerically by using the integrated model. The results presented below were compared with experimental data consisting of images of surface morphology, variation of the interface width with respect to time, and current/time curves. In addition, several key parameters were varied, and the computed results were compared with each other as well as with experimental data.

A comparison between computed and experimental data for the current/time response of the base case for various overpotentials is shown in Fig. 3. (The noise in the Monte Carlo calculations is a result of using random number to compute a statistical solution, and could be reduced by using a larger sample size for the computations.) For time greater than about 50 s, the experimental data for 50 and 150 mV compared well with the computed results. Data for 300 mV show that the experimental current was up to 18% higher than calculated values. We attribute this deviation to migration effects that are more important at higher potentials where transport processes tend to influence behavior. Although migration effects were not considered at either continuum or noncontinuum level, their ef-

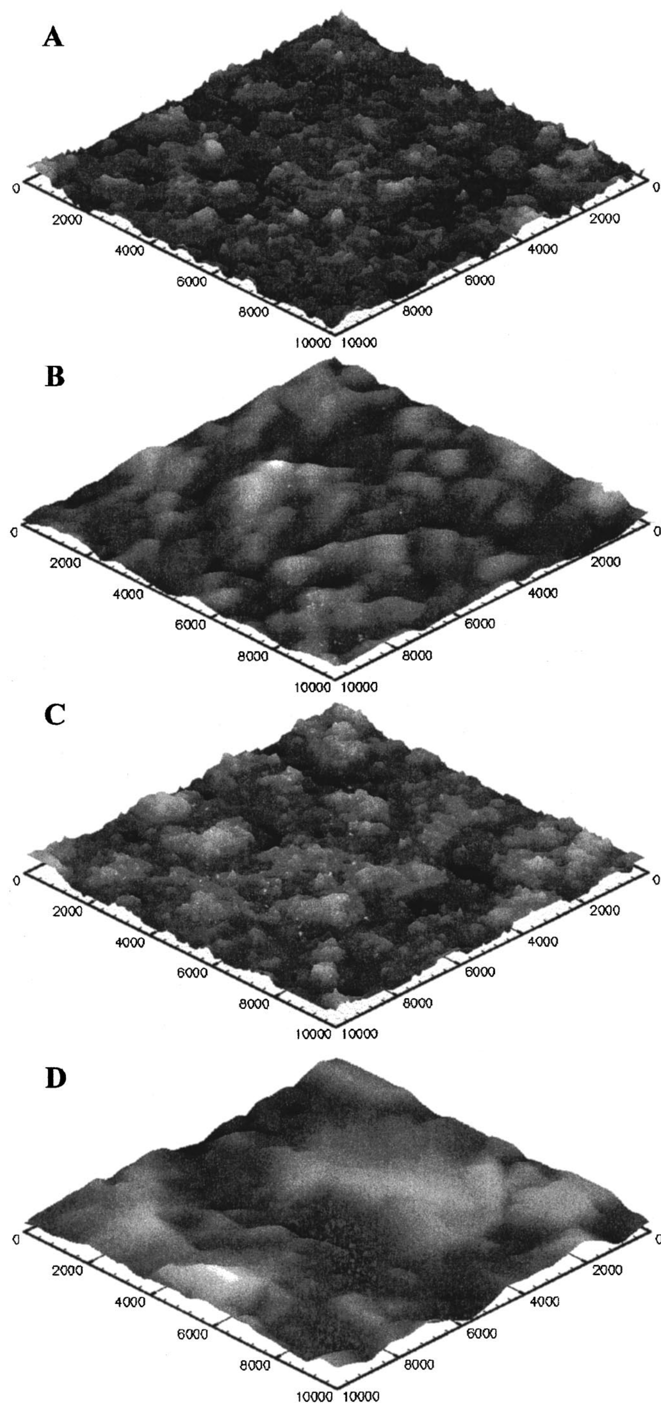

Figure 4. 10×10 μm images of surface (a) 500 s (simulated), (b) 500 s (AFM data), (c) 1000 s (simulated), and (d) 1000 s (AFM data).

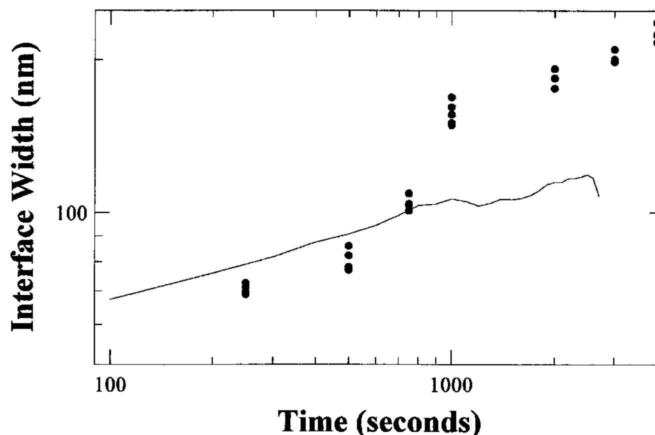

Figure 5. Scaling of the interface width for base case. Line is the results from the simulation and the circles are experimental data.

fect may be estimated[66] to fall between 10% (for the case of complete dissociation of bisulfate ions) and 30% (the case of no dissociation of bisulfate ions). At times less than 50 s the current/time curves deviated from the experimental results, probably due to nucleation effects which were ignored in the model. For the remaining discussion, emphasis will therefore be placed on data obtained at 50 and 150 mV and for times greater than 50 s since these corresponded to the situation where growth (not nucleation) occurred under surface reaction kinetic control.

Images of the simulated and experimental AFM surfaces, respectively, for deposition lasting 500 s at 150 mV are shown in Fig. 4a and b. Similar images for deposition lasting 1000 s are in Fig. 4c and d. In all figures, the image area is 10×10 μm and the z scale is the same scale as the x and y scales. The number of points in the simulation images is 100×100 and in the experimental AFM images is 256×256. Because the simulated images have about 6.6 times fewer points than the AFM images, the simulated images typically have a coarse grainy look by comparison with the experimental data. From a comparison of Fig. 4a with 4b, and Fig. 4c with 4d, an assessment of the goodness of fit may be made with respect to the nature and size of surface structures. Several types of improvements can be made to facilitate comparison between experiment and simulation. These would include methods to reduce simulation noise which is typically present in roughness simulations that have small numbers of data points, such as occurs in computing interface width at small length scales. In addition, improved methods to select (fit) values of parameters could be used. The present work, however, is adequate to look for trends as well as effects of the key parameters. For example, in the AFM image at 1000 s there is a large surface structure that is not seen on the simulated surface. Also, a trend can be seen in both the experiments and simulations of smaller surface structures growing into larger structures.

The calculated results for scaling of the interface width with respect to time for the base case at 150 mV along with experimental results are shown in Fig. 5. Each point represents a different experiment. For any particular time throughout the range investigated, the standard deviation of the experimental data was less than 5% of the average value at that time. Below 800 s, the two experimental data sets exhibited the slope $\beta = 0.19$ which was identical to slope of the simulated results over the same time scale. In the same region, the spatial scaling exponent for experimental and computed results were $\alpha = 0.97 \pm 0.02$ and $\alpha = 0.88 \pm 0.07$, respectively. These values may be compared with theoretical results based on continuum models of surface diffusion which give the values of $\alpha = 1$ and $\beta = 0.25$. At around 800 s, the experimental data shown in Fig. 5 exhibited a roughening transition. From auxiliary estimates based on the Cottrell equation, it was found that the system entered diffusion-limited behavior at about 1000 s. It is not unreasonable to suggest that scaling behavior changed as a consequence. In fitting parameters of the Monte Carlo code, we used only data below 800 s since we wished to obtain values under conditions for which there were negligible concentration gradients in the bulk solution. The simulation results did not exhibit a roughening transition when extended up to about 2500 s.

We note that while the importance of surface diffusion control above -100 mV has been questioned,[20] the results in Fig. 5 indicate that such a hypothesis may be supported for the first 500 s of electrolysis at a potential of -150 mV.

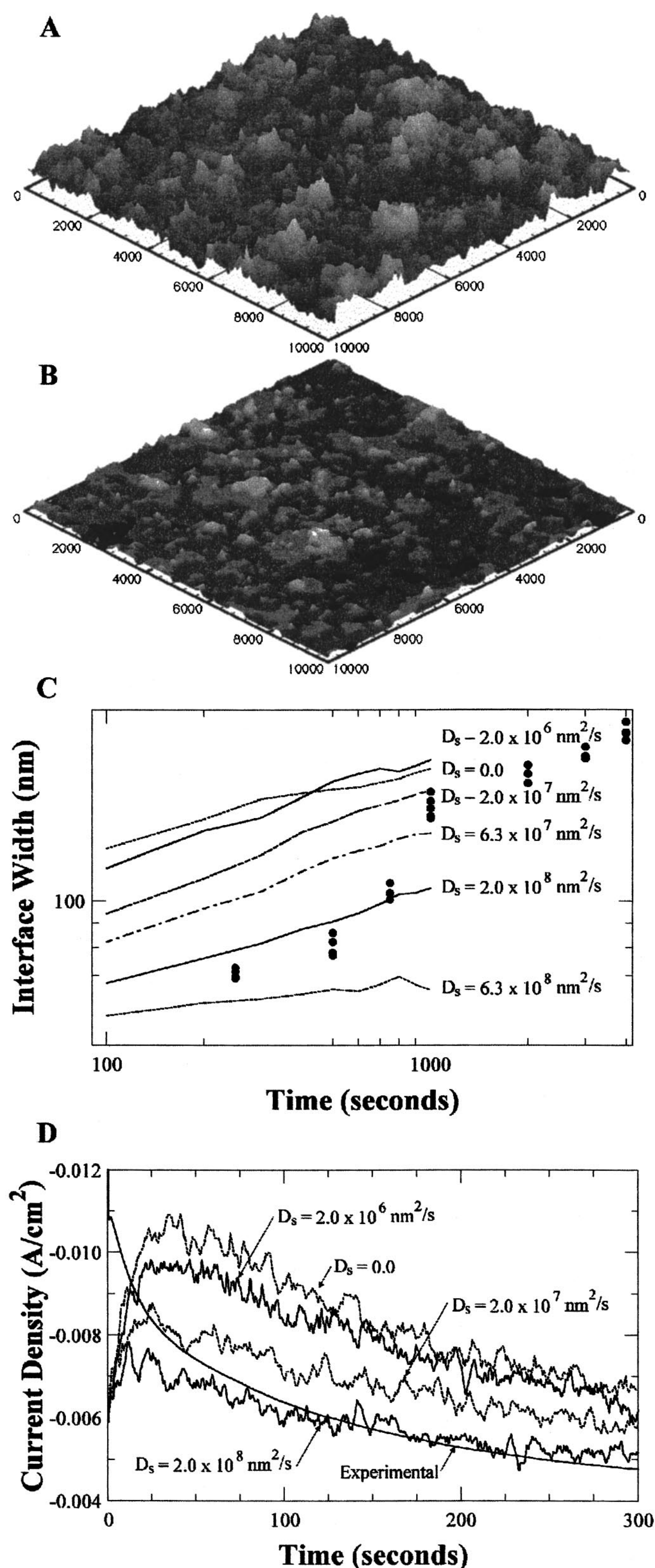

Figure 6. Effect of surface diffusion (a) 10×10 μm images of simulated surface for $D_s = 0$ after 100 s, (b) 10×10 μm images of simulated surface for $D_s = 6.3 \times 10^8$ nm^2 after 1000 s, (c) scaling of the interface width, and (d) current/time curves.

Effect of surface diffusion rate of Cu^+.—The surface diffusion rate of Cu^+ for the base case ($D_s = 2.0 \times 10^8$ nm^2/s) was modified to investigate its effect. Simulated results for several values between 2.0×10^6 and 6.3×10^8 nm^2/s, plus the limiting case of zero are shown in Fig. 6. Images of simulated surface roughness for two different diffusion rates after 1000 s of deposition can be seen in Fig. 6a and b; a third image in the sequence was given previously in Fig. 4c. By comparison of these three images it may be recognized that the surface becomes smoother as the surface diffusion rate increased, a reasonable result because more rapid diffusion allows more chances for the Cu^+ to find a site with more neighbors to incorporate into the crystal lattice. Surfaces simulated with zero and low values of surface diffusion rate were found to produce simulated deposit structures with a large number of micro voids.

The scaling of the interface width respect to time is shown in Fig. 6c. It can be seen that the surface becomes smoother with an increase in surface diffusion rate. It can also be seen that the surface roughness evolution for the value of $D_s = 2.0 \times 10^6$ nm^2/s is quite similar to behavior simulated with a zero value of surface diffusion ($D_s = 0.0$).

The effect of the surface diffusion rate on current/time curves is shown in Fig. 6d. All of the curves are seen to have a starting point of about -0.006 A/cm^2. It can be seen that decreasing the diffusion rate produced increased currents. From Fig. 6 it was seen that a lower diffusion rate led to rougher surfaces that had a higher surface area. The increase in surface area could account for the higher currents. The initial current was presumably not affected by the surface diffusion rate because the surface had not grown enough to a great enough extent to influence surface area.

Effect of diffusion over step energy barrier for Cu^+.—The step energy barrier is associated with the energy required for movement between vertical levels on the surface. The value chosen for Cu^+ in the base case was $E_s = -1.5 \times 10^{-20}$ J. Additional calculations were carried out over the range of -1.0×10^{-20} to -3.0×10^{-20} J plus the limiting values of 0 and infinity (represented by the value $-999J$ in Fig. 7). Two example images for different step energy barriers after 1000 s are shown in Fig. 7a and b. A third example corresponding to the base case is shown in Fig. 4c. These images show that an increase in step energy barrier (to more negative values) was accompanied by roughening of the surface, a result that is reasonable since the Cu^+ that adsorbs on a bump is restricted in being able to move into a valley by the difficulty of diffusing down steps. Note from these images that the step energy barrier has a strong influence on the surface morphology, controlling the growth of nearly flat to very rough surfaces.

The scaling of interface width with respect of time can be seen in Fig. 7c. Simulated results show that an increase in step energy barrier caused the surface to become rougher. The simulated scaling results for $E_s = 0$ are very close to those for $E_s = -1.0 \times 10^{-20}$; moreover, there is only a small difference between the results for $E_s = -3.0 \times 10^{-20}$ and infinity. That is, the simulated results are highly sensitive to the step energy barrier only over a narrow range of values. Additional results are also available elsewhere[51] that indicated that the spatial scaling exponent decreases with step energy barrier while the temporal increases with step energy barrier.

The effect of step energy barrier on current/time curves is shown in Fig. 7d. An increase in step energy barrier corresponds to increased currents which we attribute to the fact that a rougher surface with higher surface area produces a higher current. As was the case with the image and scaling results, the effect of E_s was confined to a narrow window between -1.0×10^{-20} J and -3.0×10^{-20}.

Effect of broken face energy barrier Cu^+.—The broken face energy barrier is associated with the energy required for the separation of two blocks on the surface during surface diffusion of one of them. The value chosen for Cu^+ in the base case was $E_b = -5.0 \times 10^{-22}$ J. Additional calculations were carried out over the range from -1.0×10^{-22} J to -1.0×10^{-19} J plus the limiting values of 0 and infinity (represented by the value $-999J$ in Fig. 8). A value

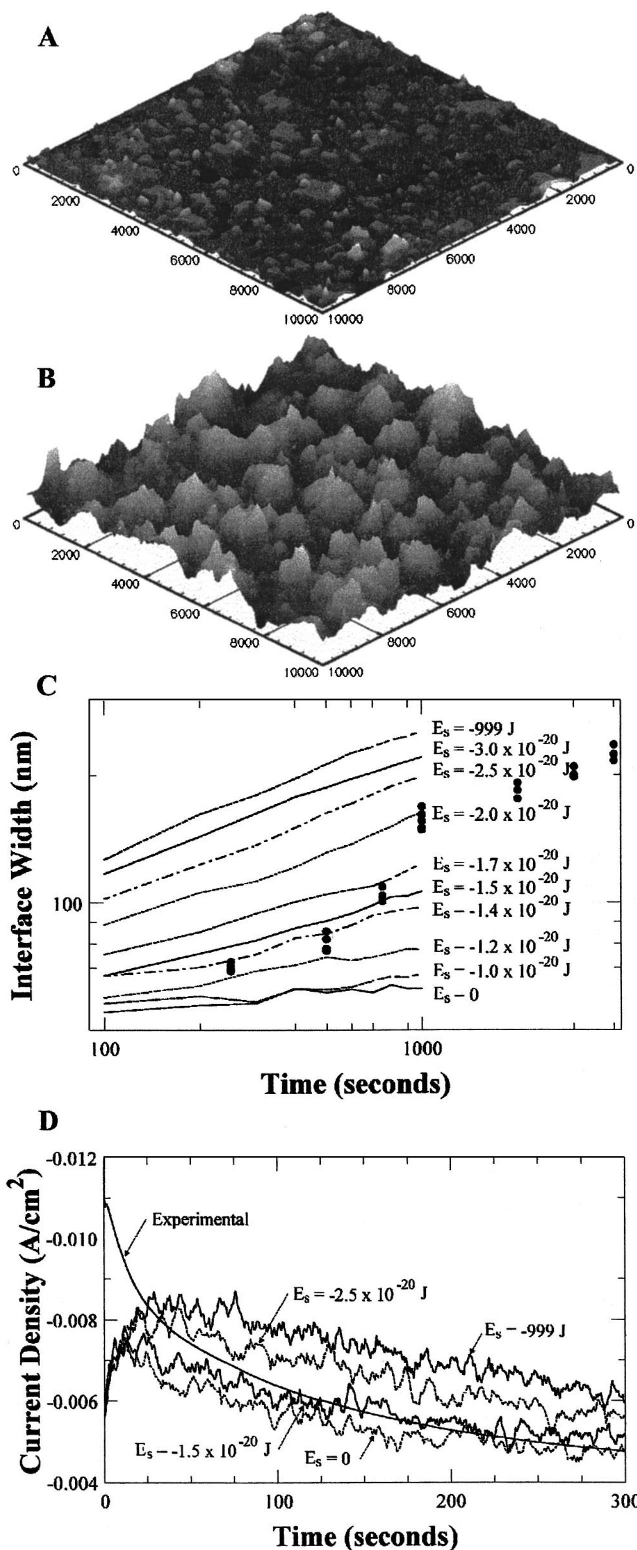

Figure 7. Effect of step energy barrier (a) 10×10 μm images of simulated surface for $E_s = 0$ after 1000 s, (b) 10×10 μm images of simulated surface for $E_s = -999$ J after 1000 s, (c) scaling of the interface width, and (d) current/time curves.

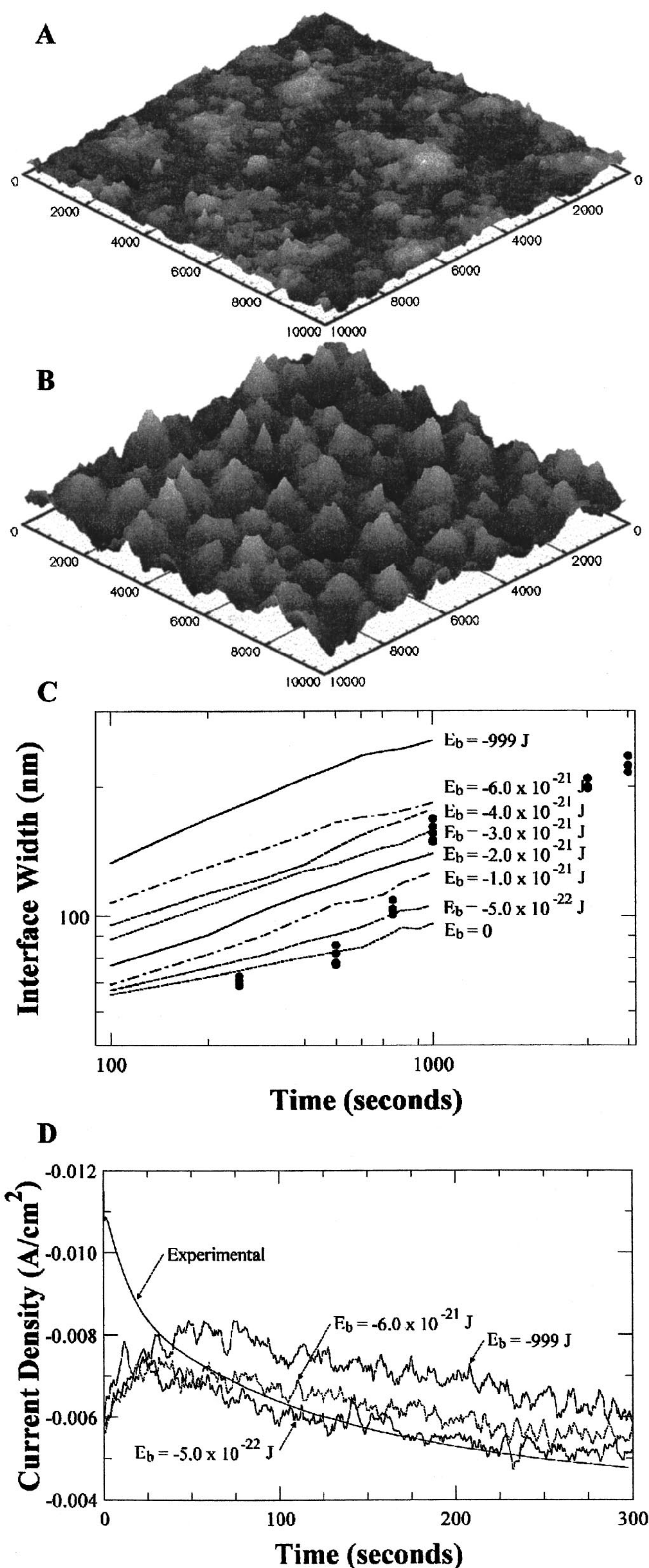

Figure 8. Effect of broken face energy barrier (a) 10×10 μm images of simulated surface for $E_b = 0$ after 1000 s, (b) 10×10 μm images of simulated surface for $E_b = -999$ J after 1000 s, (c) scaling of the interface width, and (d) current/time curves.

of infinity prevents any surface diffusion involving a broken face including step movement over and away from a step. Two surfaces for different broken face energy barriers of $E_b = 0$ and $E_b = 4$ are shown in Fig. 8 after 1000 s of deposition. A third image corresponding to the base case with $E_b = -5 \times 10^{-22}$ J is in Fig. 4a. The surface becomes rougher at the large scale and smoother in the small scale as the broken face energy barrier was increased (to more negative values). Since diffusion over a step involves a broken face,

we suggest that roughness will increase for the same reason as for an increased step energy barrier. These images show that the broken face energy barrier has strong influence on the surface morphology, controlling the growth from surfaces with little roughness to very rough surfaces. The surface roughness with no broken face energy barrier (Fig. 8a) is seen to be rougher than the simulations with no step energy barrier (Fig. 7a); we explain this observation by noting that the no broken face energy barrier simulation still has a step energy barrier.

The simulated variation of the interface width with respect to time is shown in Fig. 8c. The trend is that the surface gets rougher with an increase in broken face energy barrier (more negative values). The value of this parameter affects simulated results only in the region between $E_b = -1.0 \times 10^{-22}$ J and $E_b = -1.0 \times 10^{-19}$ J. Additional results available elsewhere[51] indicate that the spatial scaling exponent increases with broken face energy barrier, a trend that is opposite to that of the step energy barrier. We attribute this trend to the fact that small-length-scale roughness decreases with increasing energy barrier.

The effect of the broken face energy barrier on the current/time characteristics, shown in Fig. 8d, are important only for the larger, most negative, values in the range investigated. We interpret this finding to mean that small scale roughness can have a significant impact on the current/time relationship. As the broken face energy barrier was increased, there was at first a smoothing of the small-length-scale features, a trend that was reversed at larger values of the energy barrier because the energy barrier impedes movement of a step and thus causes an increase in small-scale roughening.

Effect of new face energy barrier.—The new face energy barrier is associated with the energy required for two blocks to join. The value chosen for the new face energy barrier for Cu^+ in the base case was $E_n = 5.0 \times 10^{-22}$ J. Unlike the other energy barriers, the new face barrier is positive. It has the effect of reducing the consequences of the other energy barriers when a new face is created. Additional calculations were carried out over the range from $E_n = 1.0 \times 10^{-22}$ J to 3.0×10^{-21} J plus the limiting values of 0 and infinity (represented by the value $-999J$).

Simulation results for various values of new face energy barriers are available elsewhere,[51] and are only summarized here. It was found that the surface became smoother as the new face energy barrier was increased, a reasonable trend since the new face energy barrier facilitates particle movement into sites having more neighbors. It was found that the value of the new face energy barrier can have a strong smoothing effect on the surface within the range of 1.0×10^{-22} J to 3.0×10^{-21} J. The scaling of the interface width with respect to time was found to increase slightly with the new face energy barrier (except for the limiting case of an infinite energy barrier), probably because of the smoothing effects.

Effect of reaction rate of Cu incorporation.—The value chosen for the reaction rate of incorporation of Cu according to Eq. 7 for the base case was $R_2 = 2.0 \times 10^4$ nm/s. Additional calculations were carried out over the range from 2.0×10^2 to 2.0×10^5 nm/s. Images for these calculations are available elsewhere.[51] It was found that the surface was smoothest for low values of R_2 and became rougher as the reaction rate increased. The spatial scaling exponent (α) was found to decrease with increasing reaction rate of incorporation while the temporal scaling exponent (β) increased. These trends are consistent with the fact that the surface became rougher as the reaction rate was increased. The effect of an increase in the reaction rate of Cu incorporation on the current/time curves was to produce a higher current, in part owing to the more rapid kinetics and in part to the roughening of the surface.

Effect of adsorption barrier at steps.—Some investigators have concluded that Cu^{2+} does not adsorb at kink sites but, rather, adsorbs on a plateau.[50] This aspect of the reaction mechanism was simulated by adding an energy barrier of adsorption for every additional solid surface that the Cu^{2+} particle contacted. Thus for example a Cu^{2+} particle that contacted two or three solid surfaces (a step or kink, respectively) would have a lower probability of reaction than a particle that contacted only one surface (on a plateau). The adsorption energy barrier for each additional face was chosen to be -2.0×10^{-20} J or -4.9 kT, a value that was large enough to prevent 99.2% of the adsorption at a step and 99.99% at a kink site.

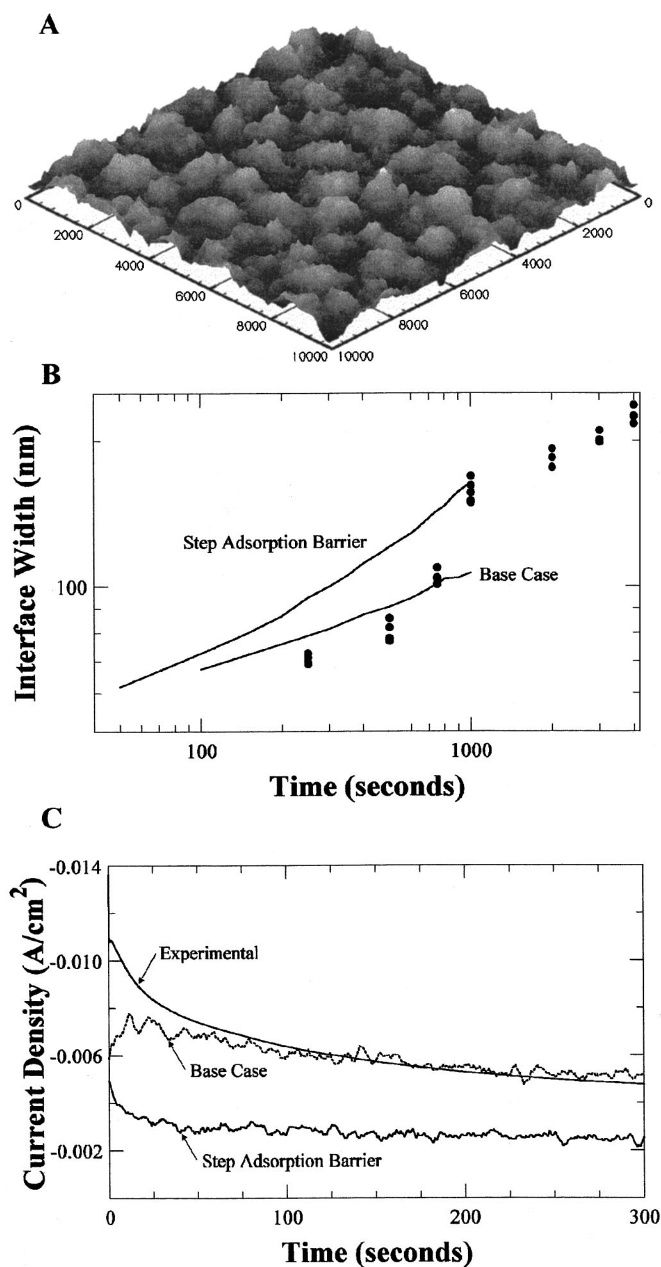

Figure 9. Effect of step adsorption energy barrier (a) 10×10 μm images of simulated surface after 1000 s, (b) scaling of the interface width, and (c) current/time curves.

A simulated surface with a step adsorption barrier after 1000 s of deposition is shown in Fig. 9a. By comparison with Fig. 4c, it is seen that the surface is considerably rougher than the base case simulations, for which there was no adsorption barrier for contact with edges and kinks. The rougher surfaces are expected when the Cu^{2+} is restricted from adsorbing in sites with many neighbors since it would otherwise tend to smooth the surface. The scaling of inter-

face width with respect to time shown in Fig. 9b shows that including the step adsorption barrier makes the surface rougher. In addition, these results are the only ones found in the parameter range investigated in the present paper where the slope of the time dependence of the interface width was not constant. The simulation with a step adsorption energy barrier produced a spatial scaling exponent of $\alpha = 0.87 \pm 0.04$ which was similar to the base case result of $\alpha = 0.88 \pm 0.07$. The effect of an adsorption barrier at steps on the current/time curve, shown in Fig. 9c, is to reduce the current, probably owing to the reduction in available surface area for adsorption owing to the greatly reduced number of available adsorption sites.

Conclusions

An integrated simulation of the evolution of surfaces during copper electrodeposition has been developed with use of a 3-D kinetic (noncontinuum) Monte Carlo model linked to a 1-D (continuum) finite difference model. The Monte Carlo part of the model addressed a reaction mechanism on and near the surface, while the 1-D part of the model addressed the diffusion of species in the bulk solution. The integrated model is capable of describing a number of mechanistic features at the solid/solution interface including adsorption, desorption, lattice incorporation, lattice dissolution, bulk diffusion, and surface diffusion. The model enables parametric investigations of the influence of fundamental physical properties, such as energy barriers, on the deposition processes as well as to compare the simulation results with experimental results.

A reaction mechanism that has been previously reported and widely investigated for the electrodeposition of Cu was used in the present work. The parameters associated with the Cu mechanism were selected to fit long term currents transients as well as evolution of interface width during roughening. The model was found to be able to simulate a number of trends associated with the electrodeposition process, as well as produce morphologies that resembled those seen experimentally.

Modifying the rate of Cu^+ surface diffusion rate had a significant effect on surface roughness evolution. Low rates of surface diffusion were found to produce rough surfaces with higher rates producing smooth surfaces. At no or very low surface diffusion rates the deposit formed micro voids. The energy barrier for Cu^+ surface diffusion over a step has a significant effect on the surface morphology. High energy barriers produce rough surfaces with low energy barriers producing smooth surfaces. Unlike the rough surfaces produced from a low surface diffusion rate, the rough surface caused from a high step energy barrier did not have a large number of micro voids. The broken face energy barrier for Cu^+ surface diffusion had a significant effect on the surface morphology. High energy barriers produce rough surfaces with low energy barriers producing smoother surfaces. Higher values for the energy barrier produced rougher surfaces very similar to those produced from the step energy barrier. The new face energy barrier for Cu^+ surface diffusion had a smoothing effect on the deposits. Higher values of the energy barrier produce smoother surfaces. Very high values are seen to have a small roughening effect by eliminating the preference to diffuse down a step compared to up a step. The addition of a step adsorption barrier was seen to produce rougher surfaces. From the scaling analysis the step adsorption barrier produced a nonlinear result similar to the experiment.

Simulations based on the proposed copper deposition reaction mechanism did not show the trend toward smoother surfaces at higher deposition rates, reported in experimental studies. Also not captured by the model were the nonlinear scaling results of the experiments at longer times when the system became controlled by bulk diffusion limitations. The approach and techniques used here show promise for the task of proposing and testing various reaction mechanisms as well as more complex deposition systems of technological interest. In Part II of this series, the effect of additive species will be considered, and the model will be extended to simulate shape evolution during deposition in small trenches.

Acknowledgments

This work was partially supported by the U.S. Department of Energy, Division of Materials Science under award no. DEFG0296ER45439 through the Frederick Seitz Materials Research Laboratory at the University of Illinois at Urbana-Champaign. The work of M.J.K. was supported by the National Science Foundation (CTS99-74962). This work was partially supported by National Computational Science Alliance under CTS970031N and utilized the NCSA SGI/CRAY Origin 2000. The assistance of T. O Drews in preparing the manuscript is gratefully acknowledged.

The University of Illinois assisted in meeting the publication costs of this article.

List of Symbols

- a transfer coefficient
- C concentration
- C_{Bulk} concentration of the bulk solution
- C_{End} concentration at end point to finite difference model in solution
- C_{MC} concentration at Monte Carlo interface to the finite difference model
- $C_{z=0}$ concentration at finite difference interface to the Monte Carlo model
- D_{b} diffusion coefficient in the bulk solution
- D_{s} diffusion coefficient for surface diffusion
- E energy barrier
- E_{s} step energy barrier
- E_{b} broken face energy barrier
- E_n new face energy barrier
- F Faraday constant
- f frequency of an action
- f_{i} frequency of an action number i
- k Boltzmann constant
- k_{rxn} reaction rate
- L_{b} length of a unit block
- n number of electrons passed in the reaction
- N number of Neighbors
- R molar gas constant
- R_2 reaction rate of Cu^+ incorporation
- T temperature
- t time
- t_{step} time step
- z distance from surface

Greek

- α transfer coefficient
- α spatial scaling exponent
- β temporal scaling exponent
- η overpotential
- ρ_{rxn} probability of an action

References

1. M. Datta and D. Landolt, *Electrochim. Acta,* **45**, 2535 (2000).
2. E. Budevski, G. Staikov, and W. J. Lorenz, *Electrochemical Phase Formation and Growth*, VCH, Weinheim, Germany (1996).
3. P. C. Andricacos, C. Uzoh, J. O. Dukovic, J. Horkans, and H. Deligianni, *IBM J. Res. Dev.,* **42**, 567 (1998).
4. P. C. Andricacos, *Electrochem. Soc. Interface,* **8**(1), 32 (1999).
5. D. C. Edelstein, J. Heidenreich, R. Goldblatt, W. Cote, C. Uzoh, N. Lustig, P. Roper, T. McDevitt, W. Motsiff, A. Simon, J. Dukovic, R. Wachnik, H. Rathore, R. Schulz, L. Su, S. Luce, and J. Slattery, Tech. Dig. Int. Electron Devices Meet., **1997**, 773.
6. R. Alkire and M. Verhoff, *Chem. Eng. Sci.,* **49:24A**, 4084 (1994).
7. R. Alkire and M. Verhoff, *Electrochim. Acta,* **43**, 2733 (1998).
8. A. S. Dakkouri and D. M. Kolb, Editors, *Electrolytic Metal Deposition: Fundamental Aspects and Applications*, Oldenbourg, Munich (1999).
9. *Electrochemical Nanotechnology: In Situ Local Probe Techniques at Electrochemical Interfaces*, W. J. Lorenz and W. Plieth, Editors, Wiley-VCH, Weinheim (1998).
10. W. Mehl and J. O'M. Bockris, *J. Chem. Phys.,* **27**, 818 (1957).
11. J. O'M. Bockris and M. Enyo, *Trans. Faraday Soc.,* **58**, 1187 (1962).
12. P. J. Hillson, *Trans. Faraday Soc.,* **50**, 385 (1957).
13. R. M. Rynders, Ph.D. Thesis, University of Illinois at Urbana-Champaign, IL (1993).
14. E. D. Eliadis, Ph.D. Thesis, University of Illinois at Urbana-Champaign, IL (1997).
15. T. J. Pricer, M.S. Thesis, University of Illinois at Urbana-Champaign, IL (1998).
16. T. Vitanov, A. Popov, and E. Budevski, *J. Electrochem. Soc.,* **121**, 207 (1974).
17. T. Hurlen, *Electrochim. Acta,* **38**, 1783 (1993).
18. Y. Ogata, K. Yamakawa, and S. Yoshizawa, *J. Appl. Electrochem.,* **12**, 439 (1982).
19. Y. Ogata, K. Yamakawa, and S. Yoshizawa, *J. Appl. Electrochem.,* **12**, 449 (1982).
20. Q. L. M. Slaiman and W. J. Lorenz, *Electrochim. Acta,* **19**, 791 (1974).
21. M. P. Allen and D. J. Tildesley, *Computer Simulation of Liquids*, Oxford University, New York Press (1990).

22. M. H. Kalos and P. A. Witlock, *Monte Carlo Methods. Part I: Theory*, John Wiley & Sons, New York (1986).
23. G. H. Gilmer and P. Bennema, *J. Cryst. Growth*, **13/14**, 148 (1972); G. H. Gilmer and P. Bennema, *J. Appl. Phys.*, **43**, 1347 (1972).
24. S. Das Sarma, *J. Vac. Sci. Technol. A*, **8**, 2714 (1990).
25. C. C. Battaile, D. J. Srolovitz, and J. E. Butler, *J. Appl. Phys.*, **82**, 6293 (1997).
26. A. C. Levi and M. Kotrla, *J. Phys.: Condens. Matter*, **9**, 299 (1997).
27. K. Shigematsu, K. Kondo, K. Hayakawa, and M. Irie, *J. Electrochem. Soc.*, **142**, 1149 (1995).
28. P. A. Rikvold, M. Gamboaaldeco, J. Zhang, M. Han, Q. Qang, H. L. Richards, and A. Wieckowski, *Surf. Sci.*, **335**, 389 (1995).
29. J. Zhang, Y. Sung, R. Rikvold, and A. Wieckowski, *J. Chem. Phys.*, **104**, 5699 (1996).
30. K. Shigematsu, K. Kondo, K. Hayakawa, and M. Irie, *J. Electrochem. Soc.*, **144**, 1340 (1997).
31. M. T. M. Koper, *Surf. Sci.*, **395**, L196 (1998).
32. R. G. Barradas and T. J. Vandernoot, J. Electroanal. Chem., **1984**, 176.
33. E. V. Albano, H. O. Martin, R. C. Salvarezza, M. E. Vela, and A. J. Arvia, *J. Electrochem. Soc.*, **137**, 117 (1990).
34. R. C. Salvarezza, C. A. Alonso, J. M. Vara, E. Albano, H. O. Martin, and A. J. Arvia, *Phys. Rev. B*, **41**, 12502 (1990).
35. R. C. Salvarezza, C. A. Alonso, and J. M. Vara, *J. Electrochem. Soc.*, **138**, 2938 (1991).
36. A. Hernandez-Creus, P. Carro, R. C. Salvarezza, and A. J. Arvia, *J. Electrochem. Soc.*, **142**, 3806 (1995).
37. P. L. Schilardi, S. L. Marchiano, R. C. Salvarezza, A. H. Creus, and A. J. Arvia, *J. Electroanal. Chem.*, **431**, 81 (1997).
38. L. Pospisil, S. Zalis, and N. Fanelli, *J. Chem. Educ.*, **72**, 997 (1995).
39. N. Fanelli, S. Zalis, and L. Pospisil, *J. Electroanal. Chem.*, **262**, 35 (1989).
40. R. F. Voss and M. Tomkiewicz, *J. Electrochem. Soc.*, **132**, 371 (1985).
41. R. D. Armstrong and S. J. Churchouse, *J. Electroanal. Chem.*, **167**, 265 (1984).
42. G. Nagy, Y. Sugimoto, and G. Denuault, *J. Electroanal. Chem.*, **433**, 167 (1997); G. Nagy, Y. Sugimoto, and G. Denuault, **433**, 175 (1997).
43. D. Y. Li and J. A. Szpunar, *Electrochim. Acta*, **42**, 37 (1997); D. Y. Li and J. A. Szpunar, **42**, 47 (1997).
44. D. Y. Li and J. A. Szpunar, *J. Mater. Sci.*, **32**, 5513 (1997).
45. A. H. Creus, P. Carro, R. C. Salvarezza, and A. J. Arvia, *Langmuir*, **13**, 833 (1997).
46. H. Shitamoto, O. Okutani, and T. Nagatani, *J. Phys. D*, **31**, 1155 (1998).
47. B. Scharifker and G. Hills, *Electrochim. Acta*, **28**, 879 (1983).
48. W. U. Schmidt, R. C. Alkire, and A. A. Gewirth, *J. Electrochem. Soc.*, **143**, 3122 (1996).
49. W. M. Tong and R. S. Williams, *Annu. Rev. Phys. Chem.*, **45**, 401 (1994).
50. J. O'M. Bockris and G. A. Razumney, *Fundamental Aspects of Electrocrystallization*, Plenum Publishing, New York (1967).
51. T. J. Pricer, Ph.D. Dissertation, University of Illinois, Urbana, IL (2000).
52. H. M. Villullas and M. L. Teijelo, *J. Electroanal. Chem.*, **384**, 25 (1995).
53. E. Herrero, J. Clavilier, J. M. Feliu, and A. Aldaz, *J. Electroanal. Chem.*, **410**, 125 (1996).
54. L. Bortels, B. Van den Bossche, and J. Deconinck, *J. Electroanal. Chem.*, **422**, 161 (1997).
55. A. Damjanovic and J. O'M. Bockris, *J. Electrochem. Soc.*, **110**, 1035 (1963).
56. K. M. Takahashi, *J. Electrochem. Soc.*, **147**, 1414 (2000).
57. H. C. Albaya and W. J. Lorenz, *Z. Phys. Chem., Neue Folge*, **81**, 294 (1972).
58. Q. J. M. Slaiman and W. J. Lorenz, *Electrochim. Acta*, **19**, 791 (1974).
59. C. K. Birdsall and A. Bruce Langdon, *Plasma Physics via Computer Simulation*, McGraw-Hill, New York (1985).
60. D. Maroudas, *AIChE J.*, **46**, 878 (2000).
61. J. Lu and M. J. Kushner, *J. Vac. Sci. Technol. A*, **19**, 2652 (2001).
62. G. A. Bird, *Molecular Gas Dunamics and the Direct Simulation of Gas Flows*, Clarendon Press, Oxford (1994).
63. R. Gomer, *Rep. Prog. Phys.*, **53**, 917 (1990).
64. W. H. Press, S. A. Teukolsky, W. T. Vetterling, and B. P. Flannery, *Numerical Recipes in Fortran: The Art of Scientific Computing*, 2nd ed., Cambridge University Press, New York (1992).
65. P. L'Ecuyer, *Communications of the ACM*, **31**, 742 (1988).
66. J. S. Newman, *Electrochemical Systems*, 2nd ed., p. 410, Prentice Hall, Englewood Cliffs, NJ (1991).